

INVESTIGATION OF INTERFACIAL STRUCTURES OF NANO-SCALE TiN/AlN MULTILAYER BY NEUTRON AND X-RAY REFLECTOMETRY

X. M. DU^{a*}, K. F. ZHENG^a, R. D. LIU^b, D. F. CHEN^b, Y. T. LIU^b,
V. I. PETRENKO^{c,e}, G. ZHANG^a, C. Q. HUANG^d, I. V. GAPON^{c,e}

^a*School of Materials Science and Engineering, Shenyang Ligong University, Shenyang 110159, China;*

^b*China Institute of Atomic Energy, Beijing 102413, China;*

^c*Frank Laboratory of Neutron Physics, Joint Institute for Nuclear Research, 141980 Dubna, Moscow region, Russia;*

^d*Institute of Nuclear Physics and Chemistry, China Academy of Engineering Physics, Mianyang 621900, China;*

^e*Physics Department, Kyiv Taras Shevchenko National University, Kyiv, Ukraine.*

Neutron reflectometry allows to characterize surfaces and interfaces of ultra-thin film layered systems down to a nanometric scale (<2 nm). It can provide a wealth of information on thickness, structure and interfacial properties in nanometer length scale. Combination of neutron and X-ray reflectometry is well suited for obtaining physical parameters of nanostructured superlattice films. In the present work nano-scale TiN/AlN multilayers with different modulation period and modulation ratio were fabricated using reactive magnetron sputtering. Neutron and X-ray reflectometry methods were used to study interface structures of multilayers. The results show that the TiN/AlN multilayers with different modulation period and fixed modulation ratio are typical superlattice films and have sharp interface between TiN and AlN layers. However, for TiN/AlN multilayers with variable modulation ratio there is the diffusion interface. It is explained that a coherent interface structure is formed in TiN/AlN multilayers, in which the metastable cubic AlN layer with the thickness of 2 nm forms as a result of the template effect of cubic TiN.

(Received November 12, 2017; Accepted April 1, 2018)

Keywords: TiN/AlN, Nano-scale multilayer, Neutron and X-ray reflectometry, Interface structure

1. Introduction

Titanium nitride (TiN) has the NaCl-type structure, possessing advantages of high hardness, high chemical stability, and excellent adhesion to substrates, which make TiN the most popular film used on cutting tools and forming molds [1-3]. Aluminum nitride (AlN) with both hexagonal and face-centered cubic crystal forms is one of the dominant high temperature materials, whose Al and N atoms are held by strong covalent bonds. It has high temperature stability and chemical stability, can still keep stable in the air under the temperature of 1000°C or in the vacuum under the temperature of 1400°C.

Nano-scale multilayers have attracted extensive attention due to its super-modulus effect and super-hardness effect. Based on Koehler theory [4], nano-scale multilayer prepared from the materials of which elastic modulus are different, such as TiN and AlN, is expected to have excellent mechanical properties. It is proved that a proper periodic modulation of two specific materials lead to a super-hardness effect. Yao [5] found that TiN/AlN multilayer with the

* Corresponding author: du511@163.com

modulation periods small than 3.6 nm possessed ultra high hardness (40 GPa) and excellent adhesion, which is applied to micro-drill for precision machining. Liew [6] had found that the TiN/AlN multilayer coated carbide tools exhibited higher wear resistance and produced better surface finish.

The interfacial microstructures of nano-scale multilayers, such as modulation period, modulation ratio and interface structure type, control the oxidation, corrosion, elemental diffusion and defect formation in interfacial zone, which seriously affect the mechanical properties and thermal stability of nano-scale multilayers. The TiN and AlN layers are alternately grown in a non-coherent interface under the suitable conditions. The diffusion between the layers is less, and the interface between the layers is possibly sharp. However, it is reported that the ultrathin AlN layer grows in metastable cubic phase under the condition of cubic crystal material template for TiN/AlN multilayers and the critical thickness limit of AlN is 2 nm [7-9]. Obviously, the presence of TiN layer in the TiN/AlN multilayers affects the growth state of the AlN layer. AlN grows in the same structure as TiN. It has very an important effect on the mechanical properties of TiN/AlN multilayer. Very few studies are reported on the interfacial structure of nano-scale TiN/AlN multilayer.

Neutron reflectometry (NR) is a powerful tool used to study surfaces and interfaces of thin films in many fields of materials. This method is used to measure the scattering length density (SLD) profile, thus the characteristics of films, such as thickness, surface roughness, interfacial roughness, composition and defects can be measured with a high spatial resolution on the nanometric scale [10-13]. For most of the ceramic multilayers, the characterization of the interfacial structure is rarely preformed by neutron reflectometry so far. Gibaud et al. [14] measured the structure along to the surface normal for ceramic-metal thin films of Pt/Al₂O₃ by neutron reflectometry, and obtained a certain periodicity which consists of blocks of Pt 28 Å thick separated by an average distance of 53 Å. In our previous study [15,16], the interfacial structure of nano-scale TiAlN/CrAlN multilayer with different modulation period was studied by neutron and x-ray reflectometry. It was found that neutron reflectivity is well suited for characterization of interfacial structure for multilayer with the small modulation period (~10 nm).

In this study, the nano-scale TiN/AlN multilayers with different modulation period and modulation ratio were synthesized by reactive magnetron sputtering. Neutron and x-ray reflectometry were used to characterize the interfacial microstructures of multilayers. The experimental results obtained in neutron and x-ray reflectometry give valuable information on modulation structure, interface structure, interfacial diffusion and interfacial mismatch of nano-scale multilayers.

2. Experimental details

2.1 Film Deposition

TiN and AlN layers were alternately deposited on the p-type Si(100) substrates with the size of 50×50 mm and thickness of 1 mm at a fixed substrate bias of -200 V using reactive magnetron sputtering. Using the high purity (both 99.99%) targets of Ti and Al, TiN and AlN films were prepared with a fixed Ar gas flow rate of 10 sccm and N₂ flow rates of 30 sccm at a DC power of 120 W. Details of the preparation process and conditions have been reported in previous work [15,16]. Through computer control, Ti and Al targets were rotated to the sputtering working position and the sputtering time was controlled. The designed structure of the multilayer samples can be represented as: Si(100) / TiN/AlN, as shown in Table 1.

Table 1. The designed TiN/AlN multilayer samples

Specimen	Film	Modulation ratio	Modulation period	Total thickness (nm)
1	TiN	-	Single layer	50
2	AlN	-	Single layer	50
3	TiN/AlN	1:1	12 nm/12 nm	240
4	TiN/AlN	1:1	15 nm/15 nm	240
5	TiN/AlN	3:1	6 nm/2 nm	240
6	TiN/AlN	5:1	10 nm/2 nm	240
7	TiN/AlN	8:1	16 nm/2 nm	240
8	TiN/AlN	1:1	5 nm/5 nm	90
9	TiN/AlN	1:1	9 nm/9 nm	90
10	TiN/AlN	1:1	15 nm/15 nm	90
11	TiN/AlN	1:1	45 nm/45 nm	90

2.2 Film characterization

Neutron reflectivity, R (the ratio between the reflected and the incident neutron intensity), was obtained on a time-of-flight multifunctional neutron reflectometer GRAINS with vertical scattering plane over the q range $0.005 \text{ \AA}^{-1} < q < 0.1 \text{ \AA}^{-1}$, where $q = (4\pi/\lambda) \sin\theta \approx 4\pi\theta/\lambda$, where θ is the fixed incident grazing angle (5 mrad) and λ is the neutron wavelength varied in the working interval of 0.8 - 8 \AA (thermal mode of the moderator at IBR-2). The specular beam was detected by a 2D position-sensitive detector (size $20 \times 20 \text{ cm}^2$, resolution $2 \times 2 \text{ mm}^2$, sample-detector distance 3 m) with the averaging of the reflected beam along the horizontal direction. The calibration against the incident spectrum was performed by a separate measurement of an empty beam (after removing the sample from the beam). The detailed structure and parameters of the GRAINS instrument can be found in work of M.V.Avdeev and co-authors [17].

X-ray reflectivity (XRR) measurements were carried out using a diffractometer (Ultima IV, Rigaku Co. Ltd.) with a rotating Cu anode x-ray source ($\lambda=1.5406 \text{ \AA}$), operating at 40 kV, 40 mA. The incident and reflected beams were collimated with slits of 0.05 mm in width and 2 mm in height and the reflection intensity was measured by a scintillation counter. The specular x-ray reflectivity, R , was measured over the Q range $0.02 \text{ \AA}^{-1} < Q < 0.14 \text{ \AA}^{-1}$. The specular reflectivity curves were recorded with a ω - 2θ scan. In addition, the grazing incidence x-ray diffraction (GIXD) on TiN/AlN multilayers also was performed to detect the crystalline structure of perpendicular to the substrate surface. The incident angle is set to 0.5° .

We used Parratt 32 fitting software from HZB Berlin to model the data [18]. The software is based on Parratt's recursive fitting algorithm [19] which allows to calculate reflectivity data for layered model systems built up from a set of well-defined layers of homogeneous refractive index and interface roughness. The neutron reflectivity profile is usually fitted using a model of the depth-dependent scattering length density (SLD) profile with nuclear component

$$\text{SLD} = \sum_i N_i(z) b_i \quad (1)$$

where the summation is over each type of atom in the system, z is the film depth, N is the in-plane

average of the number density, b is the nuclear coherent scattering length. In the case of XRR the coherent scattering length “ b ” in Eq. (1) is replaced by the Thomson scattering length for x-rays, given by: $r_e(Z + f')$, where r_e is the classical electron radius (2.818 fm), Z is the total number of electrons in the scattering atom, and f' is the dispersion term. The dispersion term for x-rays will be

$$SLD = \sum_i N_i \left(\frac{r_e}{\lambda^2} Z_i + f'_i \right) \quad (2)$$

From both XRR and NR, the depth profiles of scattering length density are obtained in a sample. Since $N_i(z)$ the number density (Eqs. (1) and (2)) remains the same for XRR and NR, in case of a multilayer with several elements, the value obtained for SLD at the interfaces from NR and XRR allows one to estimate the stoichiometry of the compounds at the interface quantitatively.

Detailed structural information for the multilayers and the interfaces was obtained in terms of three characteristic parameters: thickness, scattering length density as a function of depth and interface roughness. Errors of the parameters obtained from the fits were found to be within the range of 1.3-8.0%.

3. Results and discussions

X-ray reflectivity curves and SLD profiles on single-layer films AlN and TiN are shown in Fig.1. The corresponding SLD profiles, i.e. the SLD as a function of the direction z parallel to the surface normal of the film, are displayed in the insets. These insets provide a real space representation of the film. The reflectivity curves exhibit the characteristic Kiessig fringes. It was successfully fitted using a single layer model. The thickness of the AlN and TiN films are 59.1 nm and 46.9 nm, respectively. The obtained sputtering rate of AlN and TiN films is 0.055 nm/s and 0.031 nm/s, respectively.

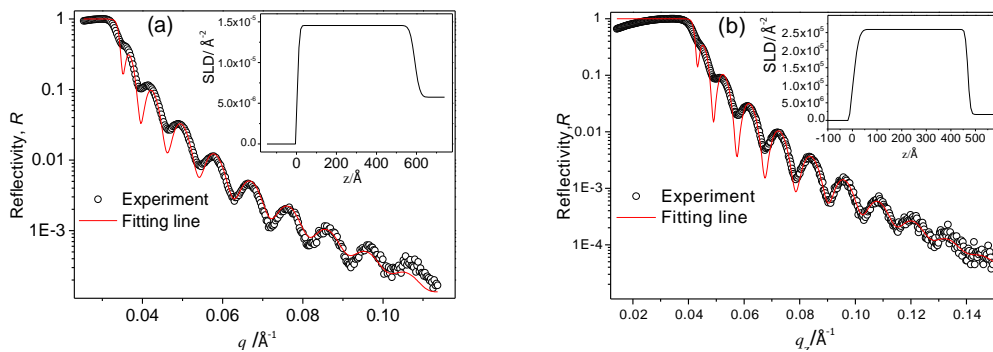


Fig. 1 X-ray reflectivity curves and SLD profiles for single-layer film, (a) AlN and (b) TiN.

Fig. 2 shows neutron reflectivity curves and SLD profiles of TiN/AlN multilayers with different modulation period thickness. Open circles and solid line are the measured neutron reflectivity data and fit to measured data, respectively. As can be seen in Fig. 2, the reflectivity curves from 12nm/12nm and 15nm/15nm TiN/AlN multilayers clearly show the presence of Bragg peaks up to fifth order and third order, respectively. It is indicated that the TiN/AlN multilayers are typical superlattice films. From the diffraction of Bragg, it is found that the periodic thickness of superlattice film can be determined according to the number of multi-level reflection at the minimum incident angle,

$$d \approx 2\pi / \Delta q_z \quad (3)$$

where d is the periodic thickness of the film and Δq_z ($q_z=4\pi\sin\theta/\lambda$) is the scattering vector difference between two adjacent reflection peaks. The average periodic thickness estimated using Eq. (3) for Sample 3 and Sample 4 is 11.6 nm and 16.3 nm, respectively. The thickness deviation between the estimated and design values is 3.3% and 8.7% for Sample 3 and Sample 4, respectively.

Parratt formalism [19] was used to calculate the reflectivity curves of the TiN/AlN multilayers (solid lines), whose parameters were perturbed in order to obtain theoretical curves that best fits the experimental data (open circles). The parameters extracted from the fit to neutron reflectometry data are summarized in Table 2. It is found that the thickness deviation between experimental and design values is 9.2% and 6% for Specimen 3 and Specimen 4, respectively. Moreover, multi-level diffraction peaks appear on the neutron reflectivity curve of TiN/AlN multilayers, indicating that the multilayers have sharp interface characteristics. This is mainly due to the non-uniform growth from cubic TiN layer and hexagonal AlN layer, which forms a sharp film interface.

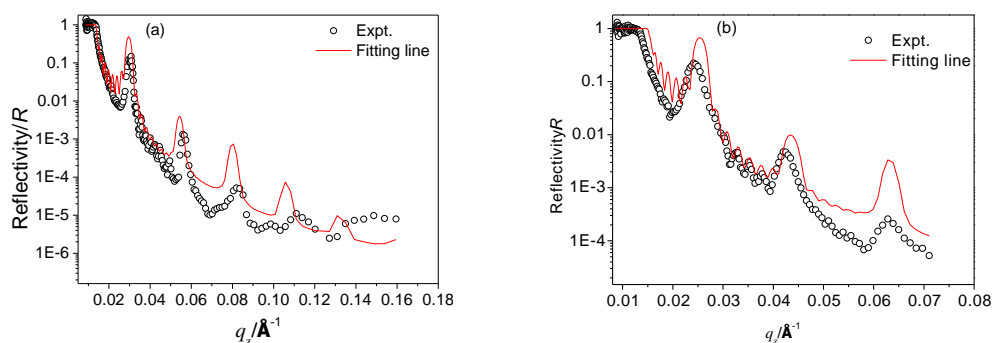


Fig. 2 Neutron reflectivity curves on TiN/AlN multilayers with different modulation period, (a) 12nm/12nm and (b) 15nm/15nm

Table 2 Fitted parameters of films from neutron and x-ray reflectometry

Specimen	Film	Thickness/nm	SLD /Å ⁻²		Roughness/nm
			Expt.	Cal.	
3	TiN	10.9	3.12×10^{-6}	3.09×10^{-6}	3.30
	AlN	10.9	6.26×10^{-6}	6.13×10^{-6}	1.30
4	TiN	15.2	3.15×10^{-6}	3.09×10^{-6}	4.60
	AlN	15.5	6.12×10^{-6}	6.13×10^{-6}	1.50
5	TiN	6.59	3.05×10^{-6}	3.09×10^{-6}	0.54
	AlN	2.15	6.23×10^{-6}	6.13×10^{-6}	0.20
6	TiN	10.0	3.13×10^{-6}	3.09×10^{-6}	1.20
	AlN	2.02	6.13×10^{-6}	6.13×10^{-6}	0.20
7	TiN	16.7	3.07×10^{-6}	3.09×10^{-6}	1.53
	AlN	2.23	6.13×10^{-6}	6.13×10^{-6}	0.30
8	TiN	5.17	1.24×10^{-5}	1.47×10^{-5}	0.85
	AlN	5.27	2.47×10^{-5}	2.75×10^{-5}	0.87
9	TiN	9.10	1.50×10^{-5}	1.47×10^{-5}	0.74
	AlN	9.06	2.67×10^{-5}	2.75×10^{-5}	0.92
10	TiN	14.9	1.71×10^{-5}	1.47×10^{-5}	1.68
	AlN	14.8	2.57×10^{-5}	2.75×10^{-5}	1.26
11	TiN	44.3	1.58×10^{-5}	1.47×10^{-5}	1.14
	AlN	43.0	2.47×10^{-5}	2.75×10^{-5}	1.36

The SLD profiles in Fig. 3 show that the fitting SLD values from experimental data are in good agreement with the calculated values (Table 2). The best-fitted SLD model for the Sample 3 shows that the SLD values for TiN and AlN layers are $3.12 \times 10^{-6} \text{ \AA}^{-2}$ and $6.26 \times 10^{-6} \text{ \AA}^{-2}$, respectively, close to their natural bulk values. Moreover, it is found that the two multilayers have typically superlattice structure in the z-direction. And the interface is very sharp. This shows that there is little diffusion between the TiN and AlN layers. The reason is that the incoherent interface is formed between the face-centered cubic TiN and the close-packed hexagonal AlN. Table 2 also shows the interface roughness of TiN/AlN multilayers. It is found that the interface roughness increases with the increase of thickness, and AlN layer is less than the roughness of TiN layer. This phenomenon can be explained by the asymmetric interface roughness on TiN-AlN-Si interfaces for studied multilayers. Generally, surface energies of the deposited layer (γ_1) and the substrate (γ_s) usually determine interface roughness. It is known that $\gamma_1 > \gamma_s$ usually causes larger interface roughness. For TiN-AlN-Si multilayer, AlN layer is first deposited on Si substrate. Next, the TiN layer is deposited on the AlN layer. So repeated, a periodic film structure is obtained.

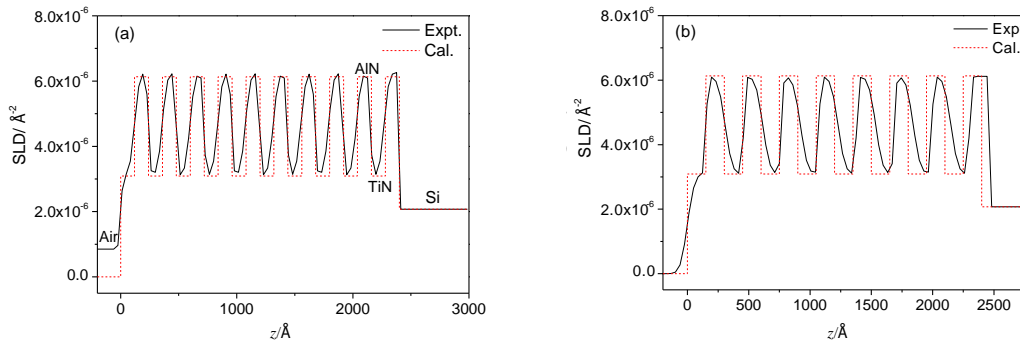


Fig. 3 The neutron reflectometry SLD depth profiles of TiN/AlN multilayers with different modulation period, (a) 12 nm/12 nm, (b) 15 nm/15 nm. The solid line denotes the fitting values and the dashed line denotes the calculated values from Eq.(1).

In order to investigate the influence of modulation ratio on the interface structure of multilayers, TiN/AlN multilayers with the modulation ratio of 3:1, 5:1 and 8:1 were also prepared. The thickness of AlN layer remains 2 nm. The thickness of TiN layer increases with increase of the modulation ratio. The neutron reflectivity curves obtained from the three specimens are shown in Fig. 4, as the open circles whereas a calculated reflectivity is shown by the solid line. The same reflectivities are shown. While the critical edge, the Kiessig fringes and the first Bragg peak remain well pronounced. The first Bragg peak shifts to lower q_z value as the modulation ratio increases, indicating increase of the periodic thickness. The reflectivity curves were fitted simultaneously to the multilayer model described above. The parameters extracted from the fitting to neutron reflectometry data are summarized in Table 2. The periodic thickness obtained from fitting for Specimen 5, Specimen 6 and Specimen 7 is 8.74 nm, 12.06 nm and 18.94 nm, respectively, which is within 10% of the desired thickness (8 nm, 12 nm and 18 nm, respectively, shown in Table 1). In particular, AlN layer with the individual thickness of 2 nm can be detected by neutron reflectometry. It is a very difficult for conventional characterization methods. Moreover, the second Bragg peak appears on the reflectivity curve of Specimen 7 (Fig. 4 (c)). That is because the thickness of the periodic thickness of Specimen 7 is larger than other specimens. This allows multi-level Bragg peaks to be observed in a smaller q_z range.

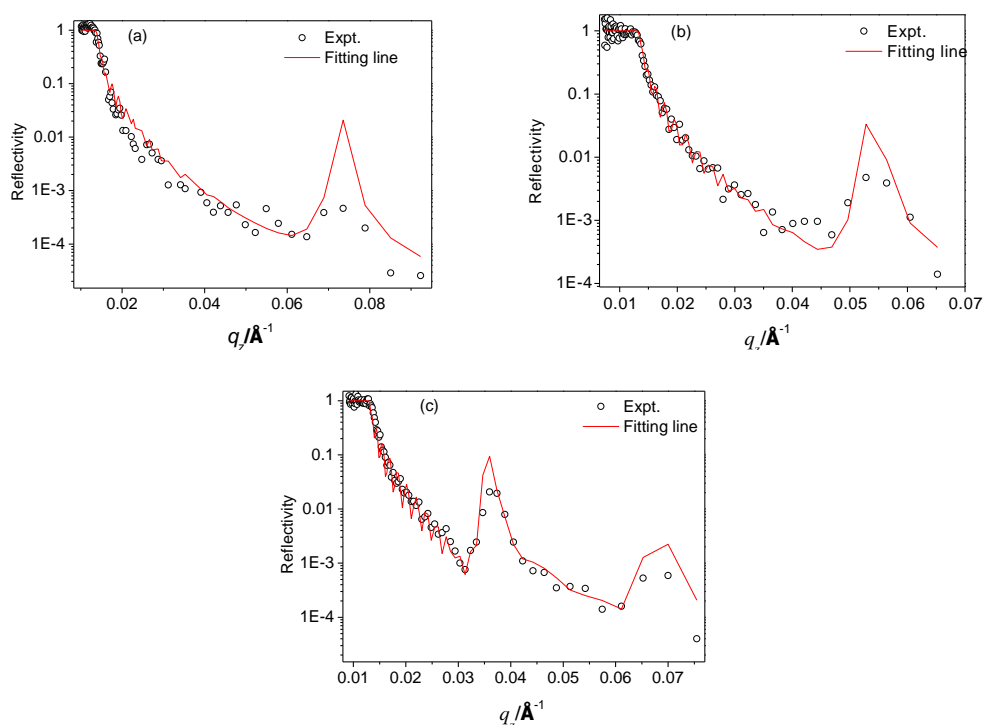


Fig. 4 Neutron reflectivity curves on TiN/AlN multilayer films with different modulation ratio, (a) 6nm/2nm, (b) 10nm/2nm and (c) 16nm/2nm.

The SLD profiles were also calculated from the mass density profile [15] shown in Fig. 5. The calculated SLD of the three multilayers is $3.09 \times 10^{-6} \text{ \AA}^{-2}$ and $6.13 \times 10^{-6} \text{ \AA}^{-2}$ for TiN and AlN layers, respectively. As can be seen, the agreement between the fitted and calculated SLD profiles for TiN layer is quite good. But this is not the case for the AlN layer. Not only the calculated SLDs deviate, to a certain extent, from the fitting SLDs, but also the width of the interface is different greatly. The main reason is that metastable cubic AlN is formed by the template effect of cubic TiN in TiN/AlN multilayers and it forms a coherent interface structure with a TiN layer through epitaxial growth. Fig. 6 (a)-(c) illustrate the grazing incidence x-ray diffraction (GIXD) from three TiN/AlN multilayers with different modulation ratio at the incident angle of 0.5° . It can be seen that three TiN/AlN multilayers possess a single-phase FCC structure, which implies epitaxial growth occurred between the AlN and TiN layers. AlN usually exists as a hexagonal structure (*h*-AlN) and may transform to a metastable cubic structure (*c*-AlN) under extremely serious conditions, such as temperature up to 1800 K and the pressure up to 14-16.5 GPa [20]. However, many researchers reported that metastable *c*-AlN can form in TiN/AlN multilayers with small modulation periods as a result of the template effect of cubic TiN and the critical thickness of *c*-AlN in the multilayers is about 2 nm [7,8,21,22]. Ultrathin AlN and TiN layers deposit alternately to form multilayer. A coherent structure is formed in TiN/AlN multilayers, which causes an increase in the interfacial width between TiN and *c*-AlN layers. In addition, the crystallization perfection of the ultrathin *c*-AlN layers in TiN/AlN multilayer is low, which causes the actual density of the *c*-AlN layer to be lower than its theoretical density. Once the AlN layer thickness increases, the epitaxial growth stops in the TiN/AlN multilayers. The metastable *c*-AlN transforms into the *h*-AlN. The TiN/AlN multilayers show a very sharp interface structure. This conclusion has been confirmed in the above neutron reflectometry experiments of Sample 3 Sample 4. Further confirmation will be made in the following x-ray reflection experiments.

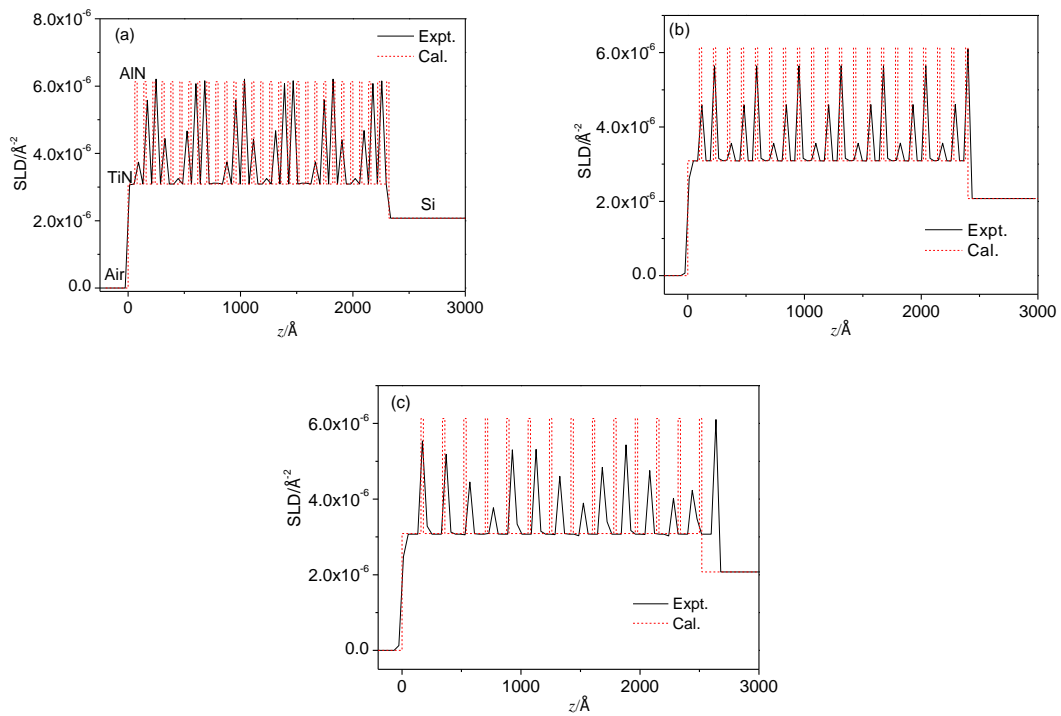


Fig. 5 The neutron reflectometry SLD depth profiles of TiN/AlN multilayers with different modulation ratio, (a) 6nm /2nm, (b) 10nm /2nm and (c) 16 nm/2 nm. The solid line denotes the fitting values and the dashed line denotes the calculated values from Eq.(1).

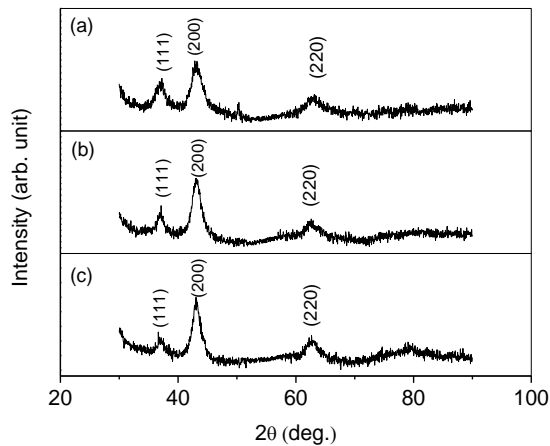


Fig. 6 The grazing incidence X-ray diffraction (GIXRD) pattern of TiN/AlN multilayers with different modulation structures at the incident angle of 0.5° , (a) 6nm /2nm, (b) 10nm /2nm and (c) 16 nm/2 nm.

X-ray reflectometry measurements were performed on TiN/AlN multilayers with the modulation period of 5nm /5nm, 9nm /9nm, 15nm /15nm and 45nm /45nm. Fig. 7 shows x-ray reflectivity curves and corresponding SLD profiles as modeled multilayer slab models for those films. The simple model is found to fit the measured reflectivity curves well. The deduced parameters, such as periodic thickness, SLD and interface roughness, from the fit to x-ray reflectometry data are also summarized in Table 2.

There exist clear multi-level Bragg peaks on reflectivity curves, as shown in Fig.7 (a)-(c), except 45nm /45nm bilayer. This indicates that these TiN/AlN multilayers are typical superlattice films, and that interface quality of the periodic bilayer becomes better as the thickness of the

periodic thickness increases. However, there is no obvious Bragg peak to be observed for 45nm /45nm bilayer, as shown in Fig. 7 (d). The reason is that the bilayer film is non-periodic. In contrast to neutron reflectometry, take 15nm /15nm multilayer for example (Fig. 2(b)), the number of Bragg peaks in Fig. 7(c) is less than that of Fig. 2(b). This is caused by the difference in the number of periodic bilayers in the two multilayers. In Sample 10, there are only three periodic bilayers, while there are 8 periodic bilayers in Sample 4. The more the periodic bilayer is, the more remarkable the superlattice feature is.

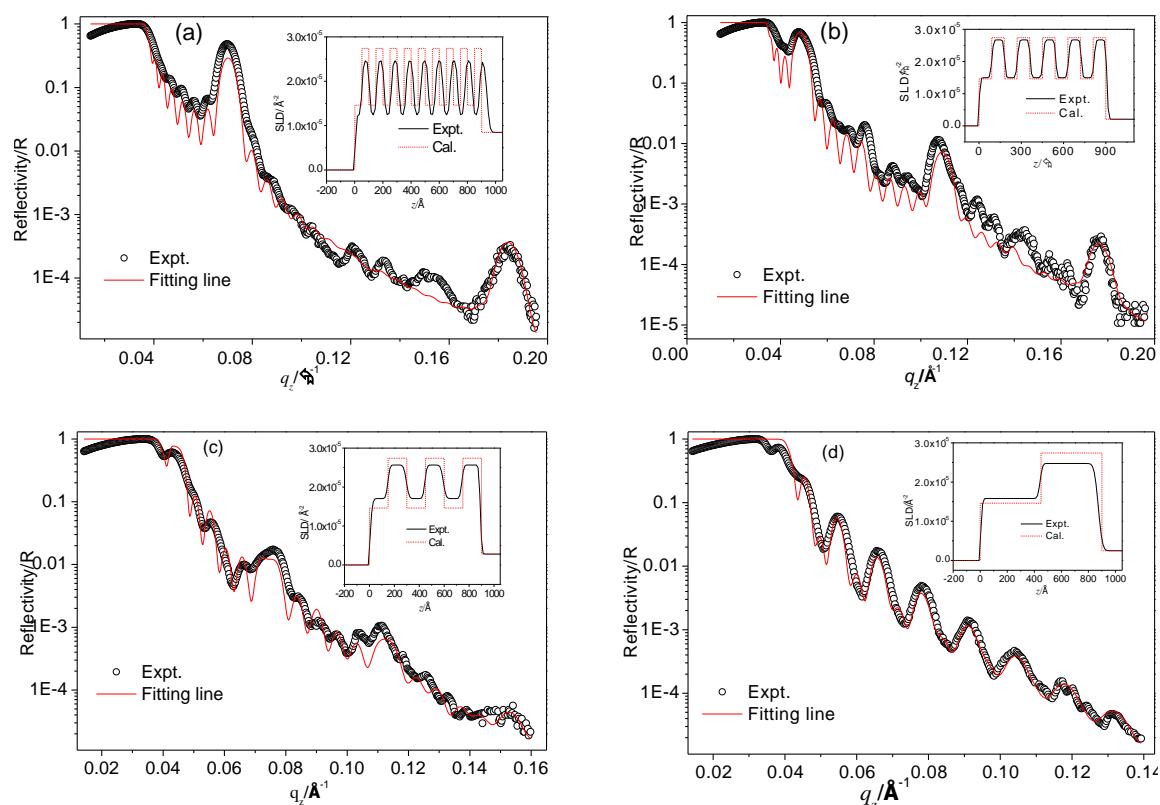


Fig. 7. X-ray reflectivity curves on TiN/AlN multilayer films, (a) 5nm /5nm, (b) 9nm /9nm, (c) 15nm /15nm, (d) 45nm /45nm

The SLD profiles was also calculated from the mass density profile [15] shown in insets of Fig. 7. As can be seen, the agreement between the fitted and calculated SLD values (Table 2) is quite good. It is also found that there exists the very sharp interface between TiN and AlN layers in multilayers. This shows that there is little diffusion between the TiN and AlN layers.

4. Conclusions

In the present work nano-scale TiN/AlN multilayers with different modulation period and modulation ratio were fabricated using reactive magnetron sputtering. X-ray and neutron reflectometry methods were used to study interface structures of multilayers. The interfacial structure parameters such as the thicknesses, the scattering length densities and interface roughness for all studied samples, were obtained by fitting experimental data to a multilayer model. The results show that the agreement between x-ray, neutron experimental reflectivity and calculated reflectivity is excellent in all cases. The TiN/AlN multilayers with different modulation period and

fixed modulation ratio are typical superlattice films and have sharp interface between cubic TiN and hexagonal AlN layers. However, there is the diffusion interface in TiN/AlN multilayers with variable modulation ratio. It is explained that a coherent interface structure is formed in TiN/AlN multilayers, in which the metastable cubic AlN layer with the thickness of 2nm forms as a result of the template effect of cubic TiN.

Acknowledgements

The authors gratefully acknowledge the financial support by NPL, CAEP (Key Laboratory of Neutron Physics, Chinese Academy of Engineering Physics) (2014BB05) and the Research Foundation of Education Bureau of Liaoning Province, China (LG201620). The authors also acknowledge User Office of FLNP JINR for organizing beam time at the neutron reflectometer GRAINS at the IBR-2 reactor.

References

- [1] J. E. Sundgren, *Thin Solid Films* **128**, 21 (1985).
- [2] M. B. Peterson, S. Ramalingam, *ASM OHIO* 331 (1981).
- [3] B. Y. Hshue, PhD dissertation, Department of Materials and Engineering, NCKU Taiwan, 1996.
- [4] J. S. Koehler, *Phys. Rev. B.* **2**, 547 (1970).
- [5] S. H. Yao, *Surf. Coat. Tech.* **197** 351 (2005).
- [6] W. Y. H. Liew, Y. G. Lu, X. Ding, B. K. A. Ngoi, S. Yuan, *Tribol. Lett.* **17**, 851 (2004).
- [7] M. Setoyama, A. Nakayama, M. Tanaka, N. Kitagawa, T. Nomura. *S Surf. Coat. Tech.* **86-87**, 225 (1996).
- [8] A Madan, I. W. Kim, S. C. Cheng, P. Yashar, V. P. Dravid, and S. A. Barnett, *Phys. Rev. Lett.* **78**, 1743 (1997).
- [9] M. Setoyama, M. Irie, H. Ohara, M. Tsujioka, Y. Takeda, T. Nomura, N. Kitagawa, *Thin Solid Films* **341**, 126 (1999).
- [10] A. K. Radzhabov, G. P. Gordeev, I. M. Lazebnik, L. A. Axelrod, V. N. Zabenkin, *Physica B* **397**, 156 (2007).
- [11] M. Dubey, M. S. Jablin, P. Wang, M. Mocko, and J. Majewski, *Eur. Phys. J. Plus* **126**, 110 (2011).
- [12] R. Kampmanna, M. Haese-Seillera, V. Kudryashov, B. Nickel, C. Daniel, W. Fenzl, A. Schreyer, E. Sackmann, J. Rädler, *Physica B* **385-386**, 1161 (2006).
- [13] M. Strobl, R. Steitz, M. Kreuzer, A. Nawara, F. Mezei, M. Rose, P. Amitesh, M. Grunze, R. Dahint, *J. Phys. Conf. Ser.* **251**, 1 (2010).
- [14] A. Gibaud, C. Sella, M. Maaza, L. Sung, J. A. Dura, S. K. Satija, *Thin Solid Films* **340**, 153 (1999).
- [15] X. M. Du, M. P. Wang, Y. Wang, X. X. Li, Z. Zhang, G. Zhang, C. Q. Huang, E. D. Wu, *Surf. Interface Anal.* **48**, 1012 (2016).
- [16] X. M. Du, M. P. Wang, Y. Wang, X. X. Li, G. Zhang, C. Q. Huang, *MRS Communications* **6**, 408 (2016).
- [17] M. V. Avdeev, V. I. Bodnarchuk, V. I. Petrenko, I. V. Gapon, O. V. Tomchuk, A. V. Nagorny, V. A. Ulyanov, L. A. Bulavin, V. L. Aksenov, *Neutron Reflectometer GRAINS with a Horizontal Sample Plane at the IBR-2 Reactor: Possibilities and Prospects*, *Cryst. Rep.* (2017) accepted.
- [18] C. Braun, *Parratt32 Software (ver.1.6)*, HMI, Berlin, 2002.
- [19] L. G. Parratt, *Phys. Rev.* **95**, 359 (1954).

- [20] P. Ravindra, S. Amin, S. Max, and J. E. Jaffe, *J. Mater. Res.* **8**, 1922 (1993).
- [21] Y. Y. Wang, M. S. Wong, W. J. Chia, J. Rechner, and W. D. Sproul, *J. Vac. Sci. Tech. A* **16**, 3341 (1998).
- [22] W. Mingshow, H. Gwoyih, Y. Shengyu, *Surf. Coat. Tech.* **133–134**, 160 (2000).